



Full Length Article

Origin and chaotic propagation of multiple rotating detonation waves in hydrogen/air mixtures

Majie Zhao, Huangwei Zhang*

Department of Mechanical Engineering, National University of Singapore, 9 Engineering Drive 1, Singapore 117576, Singapore

ARTICLE INFO

Keywords:

Rotating detonation combustion
 Reactant mixing
 Multiple detonation waves
 Chaotic propagation
 Detailed chemical mechanism

ABSTRACT

The origin and chaotic propagation of multiple detonative waves in the two-dimensional modelled rotating detonation combustor fueled by premixed hydrogen/air mixtures are numerically investigated with detailed chemical mechanism. The discrete reactants inlets are adopted, to mimic the spatial non-uniformity of the propellant in the practical Rotating Detonation Engine (RDE) combustor. The emphasis is laid on the mechanism to induce the new detonation waves in the RDE and the influence of the reactant non-uniformity in RDE on the critical detonation combustion dynamics. The numerical experiments show that the stability and number of the rotating detonation wave are affected by the inlet total pressures and reactant equivalence ratios. The RDE with high inlet total pressure would experience chaotic instability before reaching stable propagation of detonation waves in near-stoichiometric mixtures, while for the RDE with low inlet total pressure, no chaotic propagation transient after the detonation initiation is observed. It is found that the chaotic propagation stage is responsible for the variation of the rotating detonative wave number and propagation direction. Frequent detonation extinction, re-ignition and re-orientation, irregular reactants refill zones, co-rotating and counter-rotating detonation waves are observed during chaotic stage. The explosive spots arising during this stage, which may initiate new detonation waves, result from the mutual enhancement between the travelling shock waves and the deflagrative fronts. Furthermore, the predictability of the chaotic detonation wave propagation is further confirmed in terms of the initial and boundary conditions, mesh and chemical mechanism. It is also found that the fuel equivalence ratio has a considerable impact on the number of the stabilized detonation wave and velocity deficit.

1. Introduction

Rotating Detonation Engine (RDE) has revived over the past two decades since the early investigations in the middle of last century made by Voitsekhovskii [1,2], due to its promising characteristics of Pressure-Gain Combustion (PGC). Compared to the conventional deflagration-dominated combustion mode, its advantages include high thermodynamic efficiency, specific power and thrust output [3–9]. Meanwhile, compared to other types of PGC engines, such as Oblique Detonation Engine (ODE) [10–12] and Pulsed Detonation Engine (PDE) [13], RDE does not need frequently repeated fuel refilling and ignition. The fundamental physics of Rotating Detonation Combustion (RDC) relevant to RDE configurations has been studied through numerous work through theoretical analysis, experimental measurements and numerical simulations, and the latest research progress is summarized in several detailed reviews, for instance, by Wolanski [4], Anand and Gutmark [6], Kailasanath [14], Lu and Braun [3], and Zhou et al. [5].

However, due to the intrinsic complexities (e.g. multi-scale, highly transient) in RDC, up to now, there are still many unknown mechanisms which are associated with or even dominate the critical RDC dynamics, e.g. instability and multiplicity of detonation waves, fuel flexibility, efficient mixing of fuel and air, and mixed combustion modes of detonation and deflagration.

In particular, for detonation instability, it can be characterized by different phenomena, e.g. detonation pulsating propagation, quenching and re-initiation [15]. There have been numerous fundamental studies available from the literature. For instance, Short et al. [16–18] conduct theoretical analysis and numerical simulations on one-dimensional pulsating detonation and identify mechanisms for the pulsating phenomena. Radulescu and Lee study the mechanisms of detonation propagation and failure in porous-walled tubes, through revealing the evolutions of frontal structures [19]. Recently, the effects of shock tube scale, initial pressure and combustible mixture on the detonation instability have been investigated experimentally by Zhang et al. [20–22].

* Corresponding author.

E-mail address: huangwei.zhang@nus.edu.sg (H. Zhang).<https://doi.org/10.1016/j.fuel.2020.117986>

Received 3 December 2019; Received in revised form 31 March 2020; Accepted 30 April 2020

Available online 07 May 2020

0016-2361/ © 2020 Elsevier Ltd. All rights reserved.

In the context of RDE, detonation instability also has important effects on the novel unsteady phenomena, e.g. bifurcation of detonation wave and transient chaotic propagation [6], but currently their intrinsic mechanisms have not clarified yet.

This work will be focused on the origin of the dual or multiple detonation waves (for brevity, hereafter, we will term both phenomena as wave multiplicity) and their chaotic propagation before stably propagating Rotating Detonative Waves (RDWs) are achieved. Here *multiplicity* generally means the bifurcation of the detonation wave number and variation of their propagation direction (for instance, co-rotating and counter-rotating). Multiplicity of detonation waves in RDE is reported from both experimental and numerical simulations [6]. The early discussion about multiple RDWs was made by Bykovskii et al. [23,24] through his RDE experiments with various fuels for rocket motors and ramjet combustors. Based on their results, significant velocity decrease can be seen when the RDW number increases due to the increase of the propellant mass flow rate. Then RDE operation with multiple (two to nine) detonation waves have been also observed by different researchers [25–39] and a detailed summary is provided by Anand and Gutmark [6]. The factors that influence or induce the change of the RDW number include mixture reactivity (e.g. global equivalence ratio), propellant injector configuration (e.g. injector spacing), manifold stagnation pressure (or mass flow rate) and hot chamber wall surface.

The foregoing observations are mainly made through the response of the pressure signals and/or RDE imaging after regulating some quantities of interest. Nevertheless, due to the limitations of the measurement techniques, the detailed or accurate mechanism for the bifurcation of RDW number is still not clear. Meanwhile, the RDE experimental measurements (e.g. Refs. [6,27,30,38]) show that change of RDW number is always accompanied or preceded by a finitely long period with highly transient chaotic RDW propagation, which is characterized by the strong fluctuations of the measured pressure signals from RDEs. So far, it is still difficult to actively control the variations of the RDW number during this chaotic RDW propagation process towards optimizing the overall RDE performance.

In order to understand the mechanism about the formation of multiple RDWs, Wang and his co-workers conducted three-dimensional numerical simulations on RDEs fueled with premixed stoichiometric H₂/air mixture using Euler equation and one-step chemistry [40–42]. The spacing between injectors is taken into consideration in their RDE model. Their results demonstrate the new RDWs are generated from the shock waves surviving from the collisions between two counter-rotating detonative waves and also the interactions between the detonation and oppositely travelling shock waves [40–42]. In their simulations with Euler equation and two-step induction-reaction model, Teng et al. [43] find that the multiple detonation waves are formed due to the interactions between the fuel jet flow and the shock waves induced by the initial ignition. In the three- and two-dimensional simulations of H₂/air RDEs with Euler equation and induction parameter chemical model by Schwer and Kailasanath [44], the new detonation wave is caused by the ignition of the unburned reactant compressed by the shock waves, which are reflected from the nozzle exit. Through the two-dimensional simulations of H₂/air RDEs with detailed chemistry and real injection nozzles [45], Sun et al. highlight that the combustion along the contact interface between the fresh premixture and the burned gas from the last RDW cycle may induce a new detonation through interacting with the above shocks under favorable conditions.

Deng et al. explore the feasibility of mode control (i.e. number and direction of RDW) in non-premixed H₂/air RDC with Euler equations and detailed mechanism, through changing oxidizer mass flow rate, chamber length and exit blockage ratio [31]. They find that higher reactivity of the propellant would lead to its pre-combustion before the detonation front, which may develop into a detonation due to the shock wave amplification by coherent energy release mechanism. Multiple (up to four) RDWs of CH₄/air mixtures are also seen from the three-

dimensional Reynolds-averaged Navier-Stokes studies by Frovol et al. with five-step chemical mechanism [29]. In their work, re-initiation of new RDWs is attributed to the reflected shocks from the downstream outer nozzle and their interactions with the upstream refilling gas close to the head end.

Through the above numerical investigations [29,31,40,41,44,45], the propagating shock waves and the autoignition in compressed pre-mixtures are the two significant premises to induce the new detonative fronts and therefore RDWs. However, the detailed transients from localized auto-ignitive or explosive pockets in RDE flow fields to self-sustaining RDWs and the concurrent chaotic propagation stage are not investigated therein. Therefore, our understanding of the origin and subsequent evolution of new detonation waves in RDE it still needed to be improved.

In this work, we aim to investigate the transient evolutions of the detonative wavelets into RDWs and the corresponding chaotic propagation period with two-dimensional RDE model and detailed chemical mechanism for H₂/air combustion. A series of numerical experiments will be conducted through changing the stagnation pressure and reactant equivalence ratios at the upstream boundary. The emphasis is placed on the influence of the reactant non-uniformity in RDE on the critical RDC dynamics and the mechanism to induce the newly spawned detonation waves in the RDE. The rest of the paper is organized as follows: in Section 2, numerical methods and physical model are presented. The numerical results are presented and discussed in Section 3. Finally, the main conclusions drawn from our work are summarized in Section 4.

2. Governing equation and physical model

2.1. Governing equation

The Navier-Stokes equations together with the species mass fraction equations are solved for the compressible, multi-component and reactive flows, i.e.

$$\frac{\partial \rho}{\partial t} + \nabla \cdot (\rho \mathbf{u}) = 0 \quad \frac{\partial \rho}{\partial t} + \nabla \cdot [\rho \mathbf{u}] = 0, \quad (1)$$

$$\frac{\partial (\rho \mathbf{u})}{\partial t} + \nabla \cdot (\rho \mathbf{u} \mathbf{u}) + \nabla p - \nabla \cdot \boldsymbol{\tau} = 0, \quad (2)$$

$$\frac{\partial (\rho Y_m)}{\partial t} + \nabla \cdot (\rho \mathbf{u} Y_m) - \nabla \cdot [D \nabla (\rho Y_m)] = \dot{\omega}_m \quad (m = 1, \dots, N), \quad (3)$$

$$\frac{\partial (\rho E)}{\partial t} + \nabla \cdot (\rho \mathbf{u} E) + \nabla \cdot (\mathbf{u} p) - \nabla \cdot (\boldsymbol{\tau} \cdot \mathbf{u}) - \nabla \cdot \mathbf{j} = \dot{\omega}_T, \quad (4)$$

in which t is time and $\nabla \cdot (\cdot)$ is divergence operator in Cartesian coordinate. N is the number of species. The variables ρ , \mathbf{u} , E , p , Y_m , T , D , $\boldsymbol{\tau}$ and \mathbf{j} are the density, velocity vector, total energy, pressure, mass fraction of m -th species, temperature, molecular mass diffusivity, viscous stress tensor and diffusive heat flux, respectively. Note that no body forces (like gravity force) are considered in the current work. Pressure is calculated through the equation of state, i.e. $p = \rho R T$. Here R is specific gas constant of the mixture. It is assumed that the Lewis number is equal to 1, so the mass diffusivity D is calculated as $D = k / \rho C_p$, where C_p is the heat capacity at constant pressure and k is the thermal conductivity calculated using the Eucken approximation [46], $k = \mu C_v (1.32 + 1.37 \cdot R / C_v)$. Here C_v is the heat capacity at constant volume and μ is dynamic viscosity, and is predicted with Sutherland's law, $\mu = A_s \sqrt{T} / (1 + T_s / T)$, where $A_s = 1.67212 \times 10^{-6} \text{ kg} \cdot \text{m} \cdot \text{s} \cdot \sqrt{\text{K}}$ is the Sutherland coefficient and $T_s = 170.672 \text{ K}$ is the Sutherland temperature. In addition, $\dot{\omega}_m$ and $\dot{\omega}_T (\equiv \sum_{m=1}^N \dot{\omega}_m h_m)$, h_m is the formation enthalpy of m -th species) in Eqs. (3) and (4) are respectively the source terms accounting for the species generation/destruction rate and heat release rate from the chemical reactions.

The governing equations, i.e. Eqs. (1)–(4), are discretized with cell-centered finite volume method and solved by a density-based solver, *RYrhoCentralFoam*, which is developed from the fully compressible non-reactive flow solver *rhoCentralFoam* in the framework of OpenFOAM 5.0 [47]. This solver can simulate compressible flows and performs accurate shock capturing in a collocated, polyhedral, finite-volume framework using non-oscillatory central schemes. *rhoCentralFoam* itself is validated by Greenshields et al. [48] using various benchmark tests, whilst the reactive solver *RYrhoCentralFoam* has been validated for supersonic flow [49] and detonative combustion problems [50]. For the latter, in particular, good agreements are achieved about the overall behaviors of rotating detonation combustion, including the propagation speed and flow structure, as well as the cell size of the two-dimensional hydrogen-air detonation under different pressures [50].

In this work, the second-order implicit backward method is employed for temporal discretization and the time step is adjusted automatically by the solver to ensure that the maximum Courant number (i.e. CFL number) is less than 0.1 (the corresponding time step is about 10^{-9} s). Second-order Godunov-type central and upwind-central schemes following Kurganov et al. [51] are used to discretize the convection terms in Eqs. (1)–(4). Second-order central differencing scheme is applied for the diffusion terms in Eqs. (2) and (3). The chemistry-related source terms, $\dot{\omega}_m$ and $\dot{\omega}_r$, in Eqs. (3) and (4) are solved with Euler implicit method. This selection is based on our stand-alone tests of one-dimensional detonation tube using various chemistry solvers interfaced with *RYrhoCentralFoam*, including the aforementioned one and other stiff ODE solvers (seulex [52], SIBS [52] and *L*-stable embedded Rosenbrock ODE solver of order 3 [53]). Small difference can be seen from the results of the species mass fractions and temperature computed by these methods. About the computational cost, however, the Euler implicit method is about 83%, 86% and 71% faster than the seulex, SIBS and Rosenbrock solvers, respectively.

In the present simulations, detailed chemical mechanism of hydrogen oxidation (including 19 elementary reactions and 9 species) [54] is used for simulating detonative and deflagrative combustion in RDE. It has been validated in our previous work on RDE simulations [50] and used in other previous investigations [55–58]. In particular, from our previous work [50], good agreements are observed in terms of the ignition delay time (ranging from 2 atm to 64 atm) and Chapman–Jouguet (C–J) speed, through the comparisons with the corresponding experimental or theoretical data. It is found that applications of detailed chemical mechanisms are of great importance to predict the instability features of the deflagrative front between the fuel refill region and the burned gas in RDE configurations, which is also emphasized by Sun et al. [45]. This instability would further influence the dynamics (e.g. wave height fluctuation, propagation speed deficit and even self-excited instability) of the rotating detonation wave front and therefore the overall performance of the RDE [50].

2.2. Numerical set-up

A flattened two-dimensional rectangular computational domain (see Fig. 1) is used in this work to mimic that of the originally annular RDE combustor. Although some three-dimensional effects on rotating detonation propagation cannot be accounted for, such as wall boundary layer effect and lateral relief [6], however, the main characteristics of the combustion dynamics (e.g. detonation propagation) and flow patterns (e.g. shock wave evolutions) are expected to be predicted reasonably well, based on the previous two-dimensional RDE numerical investigations [59–62]. Meanwhile, it is also assumed that these three-dimensional effects are not important in the current investigations on the RDW spontaneous initiation and chaotic propagation. The length (*x*-direction) of the domain is 280 mm (equivalent to the circumference of the middle plane of 3D combustor, and the equivalent diameter is around 90 mm), whereas the height (*y*-direction) is 100 mm (equivalent to the height of the typical 3D RDE). These scales are close to those of

the practical laboratory-scale RDE chambers, such as the ones investigated by Bluemner et al. [63].

The boundary conditions are also marked in Fig. 1. The outlet is assumed to be non-reflective, which can ensure that the flows can leave the computational domain without any perturbation for the upstream flow field, including the deflagration and detonation fronts (as marked in Fig. 1). The left and right boundaries are periodic, so that the detonation waves can continuously propagate inside the domain. For the upstream boundary, fuel inlet and wall surface are alternately arranged, as schematically shown in the dashed box of Fig. 1. For the wall surfaces, no-slip, non-penetrating and adiabatic conditions are enforced. The area ratio (in two-dimensional case, reduced to length ratio) is assumed to be fixed as 2:3, i.e. 2 mm and 3 mm respectively. With this length ratio, sufficient fuel supply can be ensured, and meanwhile the effect of mixing between the premixture and the burned gas on RDW propagation becomes outstanding. It should be acknowledged that various area ratios may demonstrate different RDW behaviors [44]. However, this is beyond the scope of the current work, and will be studied in our future studies.

This configuration is introduced to model the discrete fuel injection systems used in the practical RDE burners. Addition of the solid wall surfaces between two fuel inlets may result in new features about the flow fields of RDE burner, for instance, localized recirculating flows and vitiated gas (from the last round of the detonation wave) between two fresh fuel streams, as well as reactant mixing between hot and fresh gas [40,41,44,45,64]. These would lead to significant transient characteristics related to formation of auto-igniting or explosive spots, detonation wavelets and chaotic propagation, as will be discussed in Section 3. Similar discrete inlet configuration has also been used by, e.g. Wang et al. [40,41] and Fujii et al. [65], to study the detonation propagation in the RDE model chamber.

The premixed stoichiometric H₂-air mixture is injected into the RDE chamber through 56 inlets (see Fig. 1) on the upstream boundary. The detailed structures of the reactants injector are not considered in this work, and this can avoid the extra flow characteristics, e.g. the reflective shocks from the nozzle exit [44,45], which would induce explosive pockets. The inlet conditions (specifically, pressure p_i , temperature T_i and velocity normal to the inlet v) simply depends on the relations between inlet local pressure p (extracted from the first cell in internal field near the inlet) and total pressure P_0 assuming isentropic expansion [40,41,61,66–68]. This results in three scenarios as below:

- (1) If $p \geq P_0$, then there are no reactants injected into the chamber through the individual inlets, which are treated as solid walls and no flashback can occur. Therefore, the local pressure p_i , temperature T_i and velocity v of these inlets respectively satisfy the following conditions (T is the local temperature from the internal field near the inlet)

$$p_i = p, T_i = T \text{ and } v = 0; \quad (5)$$

- (2) If $P_{cr} < p < P_0$, then the flows at the inlet are not choked, and therefore

$$p_i = p, T_i = T_0 \left(\frac{p_i}{P_0} \right)^{\frac{\gamma_R - 1}{\gamma_R}} \text{ and } v = \sqrt{\frac{2\gamma_R}{\gamma_R - 1} RT_0 \left[1 - \left(\frac{p_i}{P_0} \right)^{\frac{\gamma_R - 1}{\gamma_R}} \right]}; \quad (6)$$

- (3) If $p \leq P_{cr}$, then the flows at the inlet are choked, and therefore

$$p_i = P_{cr}, T_i = T_0 \left(\frac{p_i}{P_0} \right)^{\frac{\gamma_R - 1}{\gamma_R}} \text{ and } v = \sqrt{\frac{2\gamma_R}{\gamma_R - 1} RT_0 \left[1 - \left(\frac{p_i}{P_0} \right)^{\frac{\gamma_R - 1}{\gamma_R}} \right]}. \quad (7)$$

The critical pressure P_{cr} is calculated from the choking condition, based on the total pressure and reactant specific heat ratio,

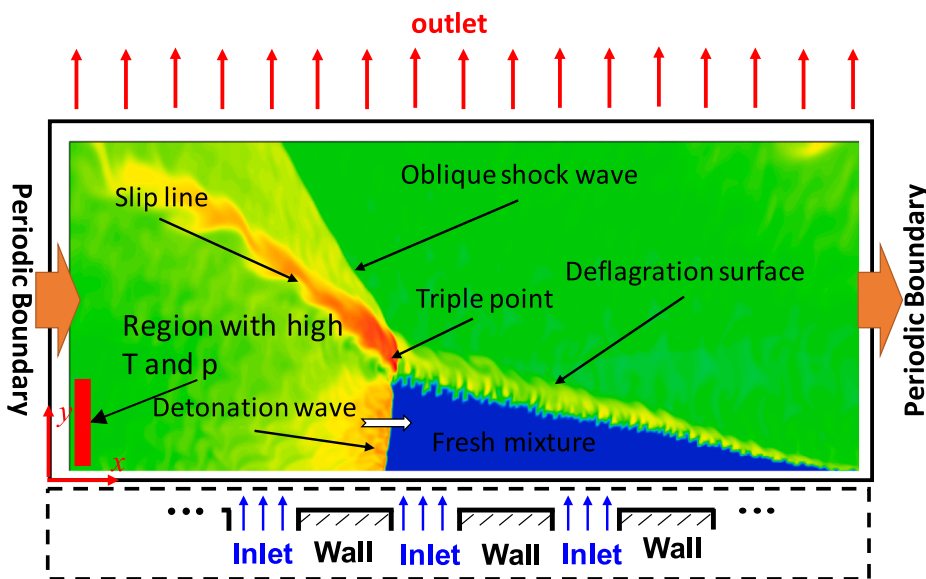


Fig. 1. Computational domain and boundary conditions in two-dimensional rotating detonation engine [50]. The red rectangular region with high (2000 K) and pressure (40 atm) is used for initiating the rotating detonation at $t = 0$. (For interpretation of the references to colour in this figure legend, the reader is referred to the web version of this article.)

$P_{cr} = P_0 \left(\frac{2}{\gamma_R + 1} \right)^{\frac{\gamma_R}{\gamma_R - 1}}$. T_0 is the inlet total temperature. γ_R is the specific heat capacity ratio of the mixture.

For the initial field (at $t = 0$), the composition of a rectangular region (280 mm \times 12 mm) closer to the inlet of the computational domain in Fig. 1 is initialized with the stoichiometric H₂-air. To initiate a propagating detonation front, a rectangular hot pocket (1 mm \times 12 mm) with high temperature (2000 K) and pressure (40 atm) is introduced at the lower left corner as shown in Fig. 1. This pocket is sufficient to generate the self-propagating detonative front in the initial field. Meanwhile, for the first cycle in which the detonative front travels towards the right side, the lateral boundaries are temporarily presumed to be non-permeable walls, to avoid the back-propagation of the detonative wave from the right side due to the initial hot pocket. This strategy can remove the shock wave counter-propagating with newly initiated detonation wave, as seen in Refs. [40,41], to achieve a stably travelling detonation front in the first cycle.

The domain in Fig. 1 is discretized with 352,800 Cartesian cells. In the x -direction, the cell spacing in the x -direction is uniform, i.e. 0.2 mm. For the y -direction, it is stretched from 0.1 mm at the inlet to 1 mm at the outlet with the stretching ratio being 10. It should be acknowledged that these resolutions are not expected to resolve the detailed detonation structures (the half reaction thickness obtained from the calculated ZND, Zeldovich-Neumann-Doring, structure is about 0.2 mm with initial temperature of 300 K and pressure of 1 atm based on the chemical mechanism given in Section 2.1 and the Shock & Detonation Toolbox developed by Shepherd and his co-workers [69]). The similar resolutions (0.1–0.2 mm) are also used in our and other two-dimensional RDE modelling work [50,60,66], in which the main RDC fields are well predicted. The sufficiency of the mesh resolution for our simulations of RDE has been confirmed in our previous work [50], through performing the mesh sensitivity analysis, and therefore will not be expanded here.

2.3. Information of the numerical experiments

The information of the simulated cases, i.e. Case 1–Case 6, is tabulated in Table 1. For all the cases, the total temperature T_0 of the reactant mixture is 300 K, and the length ratio of the inlet and wall surface is 2:3. The total pressure P_0 is increased from 5 atm in Case 1 to 30 atm in Case 6 with the increment of 5 atm. In general, the increase of the total pressure P_0 can directly lead to the increase of the inlet mass flow rates of the reactants streams [6,23].

Based on our numerical simulations, different transient behaviours

Table 1
Information of the numerical experiments.

Case	Total pressure (atm)	Transient characteristics
1	5	No chaotic propagation
2	10	
3	15	Chaotic propagation
4	20	
5	25	
6	30	

are observed after the H₂/air premixture is ignited using the hot pockets in Fig. 1, including chaotic and non-chaotic propagation of the RDWs, as listed in Table 1. Specifically, Cases 1 and 2 do not show chaotic propagation, whereas Cases 3–6 have. Additionally, all these six cases can ultimately stabilize. Phenomenologically, chaotic propagation can be characterized by the following general symptoms from our simulation results: (1) highly irregular and even disconnected reactants refill zones, (2) highly wrinkled contact surface between the fresh reactants and burned gas, (3) non-uniform propagation speed and frequency of a continuous detonation front, (4) frequent formation of new explosive spots and further evolution into new detonation waves and (5) finitely long period. These aspects are qualitatively consistent with the corresponding findings from numerical simulations (e.g. Refs. [31,44,45]) and experimental measurements (e.g. Refs. [31,37,64]).

3. Results and discussion

3.1. General RDC characteristics

In this Section, the general features of the detonation propagation in Cases 1–6 will be presented, which correspond to variable total pressures P_0 , from 5 atm to 30 atm, as tabulated in Table 1. Note that the results in this Section are extracted from the instants when the RDWs are self-sustaining and stable. Fig. 2(a)–(f) respectively show the distributions of instantaneous temperature and pressure when the RDWs are stable after a sufficiently long period. It can be seen that when the total pressure is relatively low, e.g. 5 atm in Case 1 and 10 atm in Case 2, only one detonation wave is observed, while Cases 3–6 with higher total pressure stabilize with dual detonation waves. The relation between the detonation wave number and the total pressure (or mass flow rate) has also been observed, e.g. by Suchocki et al. [35], Anand et al. [32] and Deng et al. [31]. Moreover, for these situations with dual

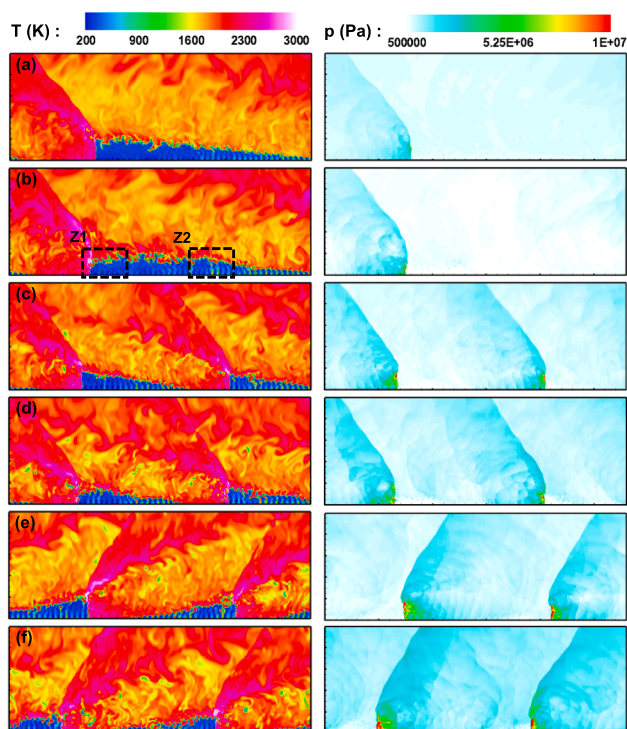


Fig. 2. Distributions of temperature (left column) and pressure (right column) when the detonation wave propagates stably in: (a) Case 1, (b) Case 2, (c) Case 3, (d) Case 4, (e) Case 5 and (f) Case 6. Z1 and Z2 are used for analysis in Fig. 3. The domain is 280 mm \times 100 mm.

detonation waves, their propagation directions are different: specifically, rightward in Cases 3 and 4, whereas leftward in Cases 5 and 6. As mentioned in Section 2.3, after the detonation is initiated using the hot spot (see Fig. 1) in Cases 3–6, they undergo a finitely long chaotic propagation stage and sometimes alternate with short stable propagation prior to ultimate stabilization. New detonative waves are formed during the chaotic propagation stage, interacting with the existing detonation and deflagration fronts alike. However, for Cases 1 and 2 in Fig. 2(a) and (b), no extra detonative combustion front is initiated, and the chaotic propagation is not observed based on our numerical experiments. The underlying mechanism and the transients of chaotic propagation will be further discussed in Section 3.2.

The propagation speed of the detonation wave in Cases 1–6 are detailed in Table 2. Here the detonation wave speed is calculated by averaging the instantaneous speed when the detonation wave propagates stably, and the instantaneous speed is determined by the propagation distance within two sufficiently short adjacent instants (about 10 μ s). The propagation speeds of double detonation waves in Cases 3–6 are around 10% lower than those with one detonation wave in Cases 1 and 2. This deviation is close to the results observed in the experiment studies [6,23,70,71]. This may be caused by the shorter mixing time in dual-wave cases than that in one-wave mode, due to the shortened

Table 2
Information on propagation of detonation waves in Cases 1–6.

Case	Total pressure (atm)	Detonation wave number	Detonation wave speed (m/s)	Deficit of detonation wave speed (%)
1	5	1	1,796	8.37
2	10		1,811	7.60
3	15	2	1,660	15.31
4	20		1,652	15.71
5	25		1,675	14.54
6	30		1,648	15.92

reactants refill zone as presented in Fig. 2.

The deficits of detonation wave speed are also presented in Table 2, in which the calculated speeds of single detonation wave and dual detonation waves in the present simulations are about 8% and 15% lower than the C–J velocity (about 1,960 m/s), respectively. Noted that the measured speeds in the experiments of practical RDE combustor [6,23,70,72] are typically about 10% to 30% lower than the C–J velocity. The reasons about the deficits of detonation wave speed can be diverse and so far it is still difficult to pinpoint the factor(s) from a specific case [6]. The fundamental studies of detonation propagation [21,73–75] suggest that the detonation velocity deficits are mainly affected by the shock tube width, shock tube wall boundary layer, axial momentum loss due to the mass flow divergence in the reaction zone and the instabilities behind detonation waves. Regarding the velocity deficits observed in RDE, some researchers attribute to, for instance, the reactants layer height, channel width, curvature of annular combustion chamber and mixture reactivity [32,33,70,76]. In our previous work using a continuous reactant injector model (without walls) [50], the detonation wave velocity deficit is about 4%, much lower than all the counterpart results in Table 2. Therefore, reactant mixing due to the discontinuous injection of fresh reactants may be responsible for the higher velocity deficits predicted from this work. This is expected to be more outstanding in RDE with separate reactant injections, where efficient fuel and oxidizer mixing is needed before the rotating detonation wave arrives [6]. The reactant mixing effects in the triangular fuel zones of Cases 2 and 4 will be further discussed in Figs. 3–5 below.

Fig. 3 shows the enlarged distributions of instantaneous temperature, Heat Release Rate (HRR) and H_2 mass fraction gradient ($|\nabla Y_{H_2}|$) in two regions from Case 2, which are denoted by “Z1” and “Z2” in Fig. 2(b). They respectively visualize the details close to and far from the detonative front. It can be seen that the hot product gas from the last round of the detonative combustion is trapped and recirculated near the wall surface between the two neighboring fresh reactants streams, which is also observed in Refs. [31,44,45]. Therefore, mixing between the hot products and the cold premixed gas would occur. Meanwhile, the extent of the mixing of these fresh and burned gas shows considerable distinctions, even in the same reactants refill layer before the travelling detonative wave, e.g. in Fig. 2. For instance, closer to the detonative front, longer residence time of the reactants in the combustor can be expected, and relatively spatially uniform temperature (< 400 K) is demonstrated in Fig. 3(a₁). Nevertheless, in Fig. 3(b₁), more upstream with respect to the detonation front, higher temperature is seen in the ribbon-shaped recirculation zone near the wall. These zones are also connected with the deflagrative front, along which the isobaric combustion proceeds. It should be noted that the two-dimensional nature of the present simulations would exaggerate both the strength and effects of trapped products in these recirculation zones. However, the results can still provide insights for the effects of discrete inlets, which are more representative of actual RDE devices.

Meanwhile, the spatial inhomogeneity of the reactants can be quantified through the distributions of the fuel gradients $|\nabla Y_{H_2}|$ in Fig. 3(a₃) and (b₃). Besides the considerable $|\nabla Y_{H_2}|$ along the wrinkled deflagrative fronts, they are also present and alternately appear along the interface between the reactants and hot product gas, which is generally perpendicular to the detonation propagation direction. The latter is not seen in our previous simulation [50] with continuous reactants inlet along the upstream inlets. Like the temperature distributions in Fig. 3(a₁) and (b₁), the fuel gradients are more pronounced in Fig. 3(b₃) due to the shorter residence time to achieve better reactant mixing.

The above spatial features of temperature and reactant composition lead to the distorted detonative front and non-continuous heat release along it. For instance, in Fig. 3(a₂), the detonation wave is 3-shaped, and the heat release rate along this front varies considerably. As it propagates, the front would have variable instantaneous shape and heat release intensity, depending on the local mixing between the fresh

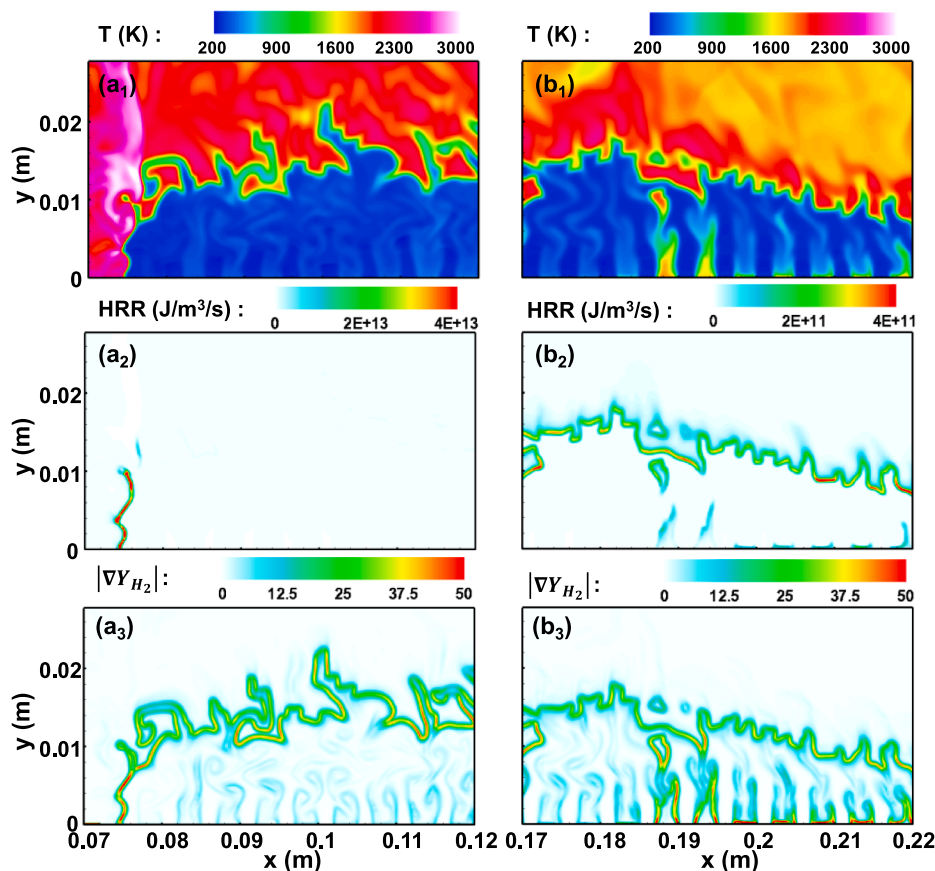


Fig. 3. Distributions of temperature, heat release rate and H_2 mass fraction gradient of two regions in Case 2 marked in Fig. 2(b): (a_1, a_2, a_3) are for zone “Z1”, whilst (b_1, b_2, b_3) for zone “Z2”.

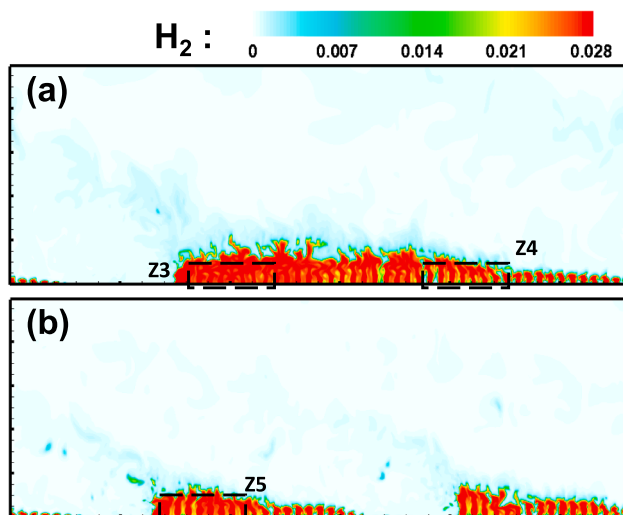


Fig. 4. Distributions of instantaneous H_2 mass fraction for (a) Case 2 and (b) Case 4. Z3-Z5 will be used for analysis in Fig. 5. The domain is $280 \text{ mm} \times 100 \text{ mm}$.

reactants and burned gas. Accordingly, the height (i.e. y direction) of the detonative front also frequently varies, thereby inducing unstable propagation. These features are not observed from the results from RDE modelling with uniform reactant injection [50,61,66].

Discussed in Fig. 3 are the disparities of the fuel mass fraction, temperature and heat release rate in Case 2 with single detonation front. To elucidate the mixing effects on the RDWs when the wave number changes, Fig. 4(a) and 4(b) compare the distributions of

instantaneous H_2 mass fraction for Case 2 and Case 4, which have one and two detonative waves, respectively. The distribution of H_2 mass fraction immediately in front of the detonation wave (e.g. in the dashed boxes) in Case 2 is more uniform than that in Case 4. This is consistent with Fig. 3(a_3) and (b_3). Unburnt H_2 can be observed after the detonation wave and near the slip line in Case 4.

Fig. 5 shows the scatter plots of instantaneous temperature versus H_2 mass fraction in the three dashed zones, i.e. Z3, Z4 and Z5, in the fresh reactants layer for Cases 2 and 4. They are colored by the reaction progress variable c , which is calculated as $c = Y_{H_2O}/Y_{H_2O}^{max}$. Here $Y_{H_2O}^{max}$ is the maximum value of H_2O mass fraction in the entire RDE combustion chamber. $c = 1$ means complete reaction, whereas $c = 0$ indicates no reactions. For zone Z3 from Case 2 with one detonation wave, most of the local hydrogen mass fractions are close to or slightly smaller than 0.0283, which corresponds to the stoichiometric H_2 -air. Meanwhile, the local temperatures of most scatters are lower than 500 K and the reaction progress variable is approximately zero. For zone Z4 that is relatively farther from the detonation front, the scatters span within the whole ranges of H_2 mass fraction and temperature. Considerable chemical reactions are demonstrated with $c > 0.75$ and $T > 1800 \text{ K}$. Therefore, in the same reactants layer supporting one detonative wave, the closer the reactants premixture to the detonation wave, the better mixing between reactants and vitiated gas, and the lower the reaction progress is.

For Case 4 with dual detonation waves presented in Fig. 5(c), there are large amounts of scatters with H_2 mass fractions lower than the stoichiometric value 0.0283. Also, the temperatures range from 300 K to 1600 K, which respectively corresponds to the temperature of the fresh reactants premixtures and the hot product near the wall. Therefore, mixing between the premixed reactants gas and the hot product is not well performed. Moreover, in Case 1, limited reactions occur in

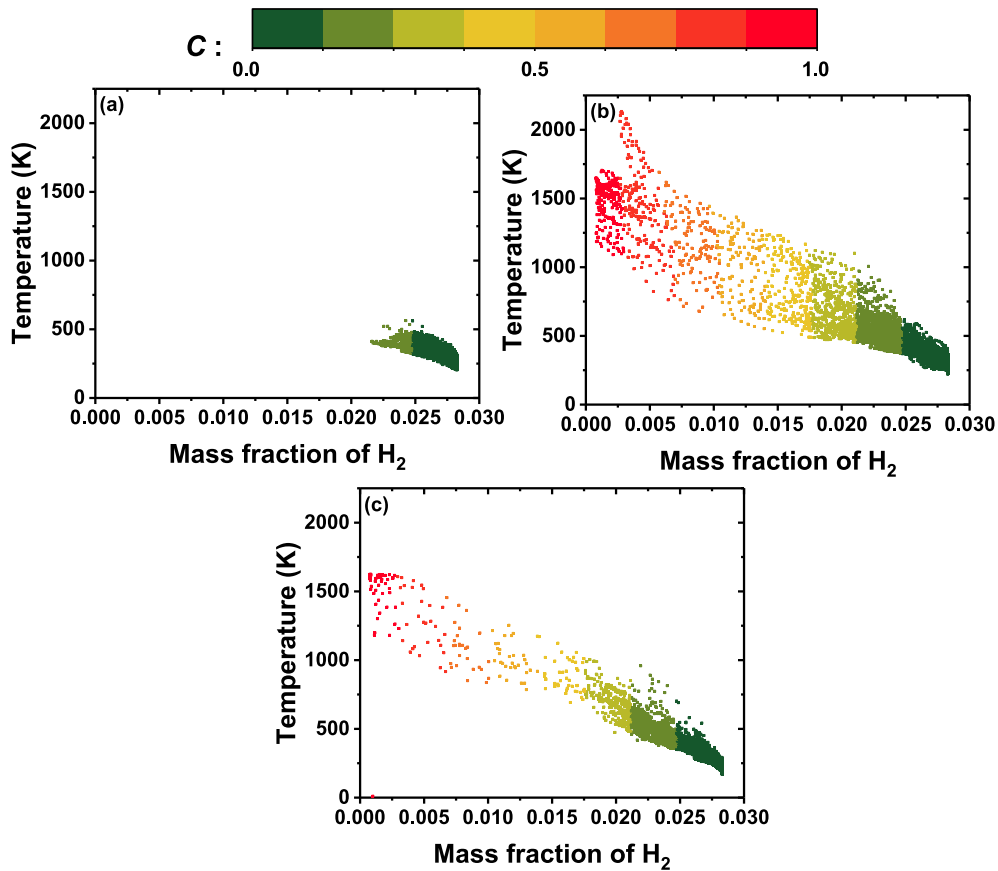


Fig. 5. Scatter plots of instantaneous temperature versus hydrogen mass fraction in dashed boxes in Case 2 and Case 4 in Fig. 4: (a) Z3, (b) Z4 and (c) Z5. These scatters are colored by the normalized reaction progress c .

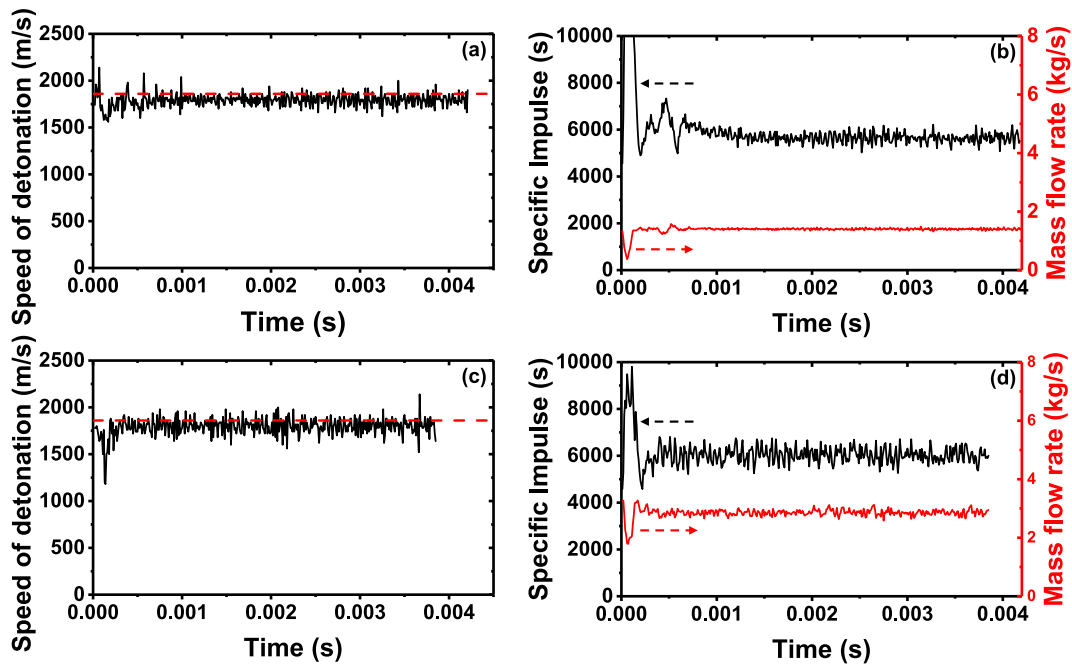


Fig. 6. Time history of detonation propagation speed, mass flow rate and specific impulse for (a, b) Case 1 and (c, d) Case 2. The red dashed lines in (a) and (c) represent the C-J velocity. $t = 0$ s corresponds to the detonation initiation instant. (For interpretation of the references to colour in this figure legend, the reader is referred to the web version of this article.)

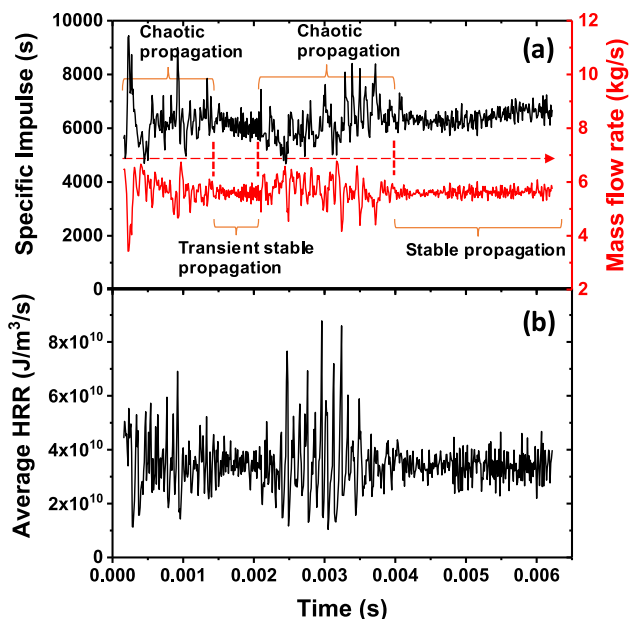


Fig. 7. Time history of (a) specific impulse and mass flow rate, and (b) volume averaged heat release rate for Case 4. $t = 0$ s corresponds to the detonation initiation instant.

zone Z5, manifested by the low c in Fig. 5(a). This is due to the relatively low local temperature, which results from the better mixing between the fresh and burned gas in front of detonation wave for Case 4.

3.2. Transient analysis on chaotic RDW propagation

The time series of instantaneous detonation propagation speed, mass flow rate ($\dot{m}_R = \int_{A_i} \rho u dA_i$) and specific impulse

($I_{sp} = \int_{A_o} [\rho u^2 + (p - p_b)] dA_o / g \dot{m}_R Y_{H_2}^o$) for Case 1 and Case 2 are respectively shown in Fig. 6(a)–(d). Here A_i and A_o are the area of all the reactants inlets and outlet, respectively, g is gravity acceleration, $Y_{H_2}^o$ is the hydrogen mass fraction in the stoichiometric H_2 -air mixture and p_b is the backpressure. Recall that both cases only have one detonation wave. Their respective propagation speeds (1796 m/s and 1,811 m/s, respectively) are slightly smaller than the C–J velocity, as confirmed by the deficits, i.e. 7–8%, from Table 2. This indicates that the statistically stable propagation of the single detonation wave can be achieved after the initial transient. Nevertheless, the propagation speeds of both cases also demonstrate considerable high-frequency and low-magnitude fluctuations (4.0% and 5.4%, respectively). The magnitudes in Case 2 are slightly larger with increased total pressure P_o . Based on Fig. 6(b) and 6(d), the specific impulse and inlet mass flow rates from Cases 1 and 2 tend to be constant also with various levels of fluctuations after the initial transition, which becomes more obvious with increasing pressure from 5 to 10 atm. Their time-averaged specific impulse is close, whereas the averaged inlet mass flow rate in Case 2 is almost doubled compared with that in Case 1. This is consistent with the observations from our previous work [50].

Different from stable detonation propagation in Cases 1 and 2, chaotic detonation propagation is found after the detonation is initiated in Cases 3–6. Plotted in Fig. 7 are the time series of mass flow rate, specific impulse and heat release rate for Case 4. It can be seen that the RDWs experience two chaotic propagation stages (marked in Fig. 7) prior to the final stable propagation, between which is a relatively short stable detonation stage (see Fig. 7). Based on Fig. 7, the two chaotic stages are characterized by the considerable fluctuations of specific impulse and mass flow rate, which have much larger magnitudes than those in the two neighboring stable propagation periods. Meanwhile, when the RDW propagates chaotically, frequent shift between high and low heat release rates can be seen from Fig. 7(b). This may imply the highly unsteady process of detonation extinction and re-ignition in the chaotic stage. These spiky HRR in Fig. 7(b) may correspond to the generation of the localized explosive spots in the reactants refill zone,

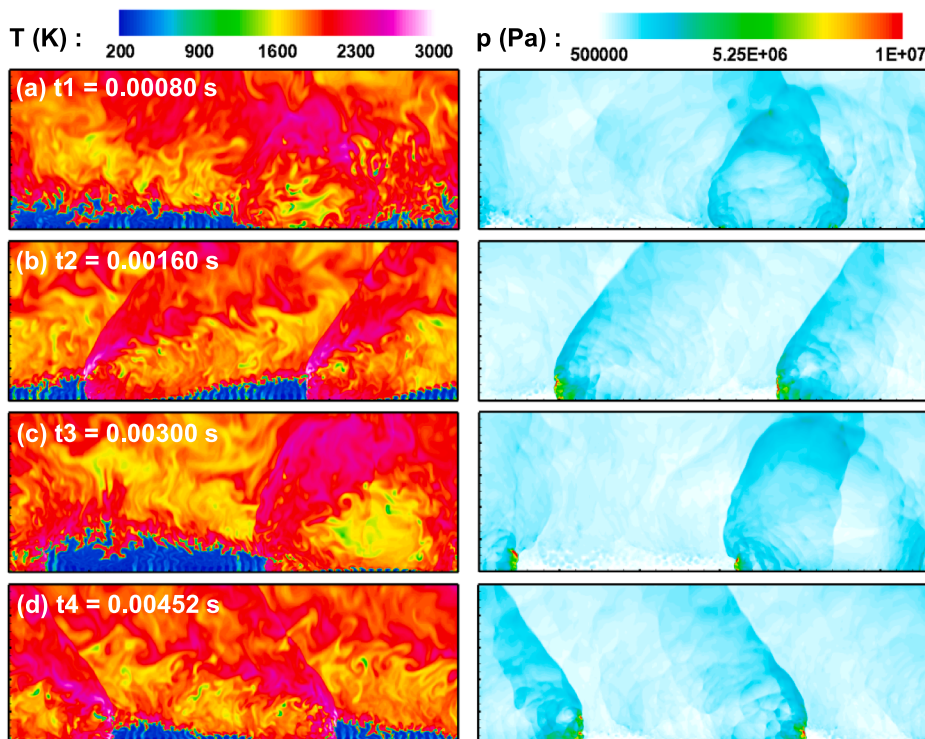


Fig. 8. Distributions of instantaneous temperature and pressure for Case 4 with four propagation stages after initiation: (a) first chaotic propagation, (b) transient stable propagation, (c) second chaotic propagation and (d) stable propagation. The domain is 280 mm \times 100 mm.

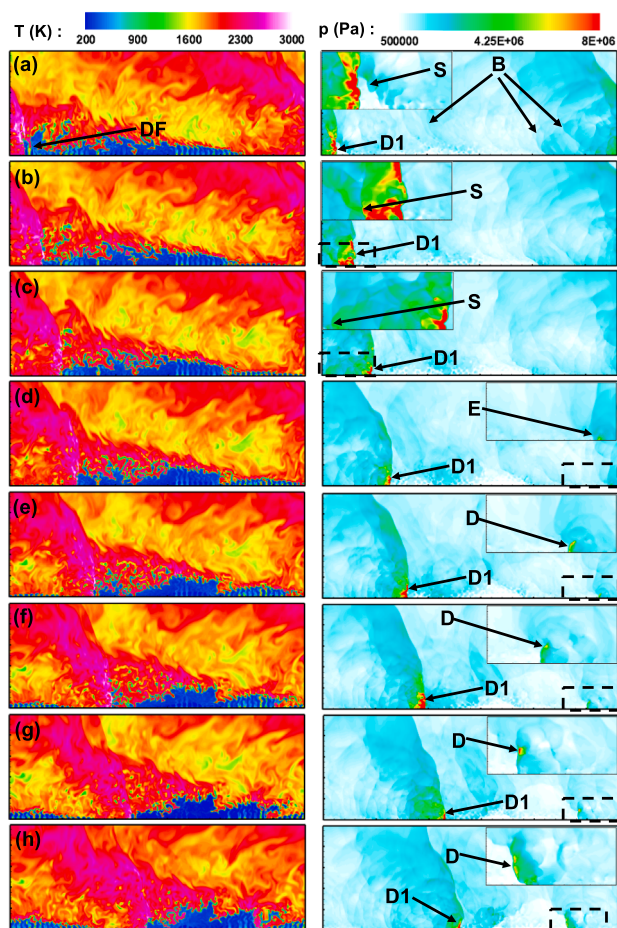


Fig. 9. Time sequences of temperature and pressure in chaotic propagation stage from Case 4. The first frame in Fig. 9(a) correspond to $t = 0.00067$ s and the time interval is 0.00001 s. D denotes detonation wave, S is shock wave, DF denotes deflagrative front, E is explosive pocket, B denotes blast wave induced by the original detonative wave $D1$. The domain is 80 mm \times 100 mm.

whereas the low values indicate the instants when the detonation wave is weakened or even quenched. This will be further shown in Figs. 9 and 11.

To further understand the detonative combustion dynamics during the four different stages (i.e. first chaotic propagation, transient stable propagation, second chaotic propagation and ultimate stable propagation) shown in Fig. 7, the temperature and pressure distributions respectively from four instants in these respective stages are presented in Fig. 8. As shown in Fig. 8(a), fresh reactants layer (visualized by low temperature) becomes not regular and strong wrinkling can be seen along the deflagrative surfaces between the burned and unburned gas. No detonation waves are observed at this instant and they may have been quenched after the collision of two counter-propagating detonation fronts, which generates two degraded shock waves. This can be confirmed by the pressure contour in Fig. 8(a). Detonation re-initiation occurs in the burner and the propagating waves stabilize around $t = 0.0016$ s shown in Fig. 8(b). Transition from chaotic propagation to stable propagation is expected to happen between $t = 0.0008$ s and 0.0016 s. In the stable propagation stage shown in Fig. 8(b), the flow fields become more organized, and two co-rotating detonative fronts exist. Nevertheless, at $t = 0.002$ s, the second chaotic propagation stage arises, which is shown in Fig. 7(a). Two counter-rotating detonation fronts are observable at $t = 0.003$ s in Fig. 8(c). Final stabilization is achieved at $t = 0.00452$ s in Fig. 8(d). Similar to the first stable propagation stage (0.0015 s $< t < 0.002$ s), double detonation fronts are seen, but they propagate towards the different direction from that in

Fig. 8(b).

As mentioned above, explosive pockets may arise and further evolve into propagating detonation waves during the chaotic propagation period. Fig. 9 shows the representative time sequences about how a detonative spot is generated in a rotating detonative field. Note that in Fig. 9(a) initially there is only one right-propagating detonation wave $D1$. Before $D1$, there is an oppositely propagating shock wave S . Based on the time sequences of the pressure field (not shown here), the shock wave S is one of the blast waves B and originally generated from the triple point from the last cycle [50], which connects the detonation front $D1$, oblique shock wave and deflagrative surface. Furthermore, the blast waves have the opposite propagation direction with respect to the detonation wave $D1$. It should be highlighted that intense deflagration combustion is also observed in this region, marked as DF in Fig. 9(a), which may interact with the shock wave and mutually enhance each other. The shock wave S is significantly intensified after colliding with the detonation wave $D1$, which can be seen in Fig. 9(b) through the high local pressure and temperature. From Fig. 9(c) and (d), the shock wave is gradually weakened (reduced post-shock pressure), but the temperature after the shock wave is still as high as 2000 K, due to the local product gas.

In Fig. 9(d), the shock wave S re-enters the domain due to the periodic boundary and a hot pocket E is formed. Fig. 10 show the details about the development of the hot spot E behind the shock wave S in the dashed box of Fig. 9(d). In Fig. 10(d₀), whose time instant is consistent with that of Fig. 9(d), a localized explosive spot, E , arises in the shocked gas and along the deflagrative interface $DF1$ (marked in Fig. 10d₀). Local high pressure and therefore large gradient (dense pressure isolines shown in Fig. 10d₀) is observed around this spot. After 10^{-6} s in Fig. 10(d₁), this spot gradually grows and intensifies the chemical reactions and therefore the heat release along the neighboring deflagrative interface $DF2$. A small section of $DF2$ further evolves into the detonative combustion. Along the y direction, this new detonative spot D is quickly extended along $DF2$, leading to a detonative front in Fig. 10(d₂). Meanwhile, based on Fig. 10(d₁) and (d₂), the upstream part (close to the inlet plane, i.e. $x = 0$) of the new reaction front is accelerated due to the locally higher temperature and pressure, and gradually approaches the leading shock wave S . The coincidence of the two fronts occurs and the left propagation detonation wave D is ultimately formed. Its subsequent development can be seen in Fig. 9(f)–(h).

The overall direction of the new detonation wave D is mainly affected by that of the shock wave S , and actually would also be adjusted based on the local reactant availability and composition, flow fields, and turbulence if in three-dimensional situations. In our previous work [50], the blast waves from the triple point is also observed in the same configuration as that in Fig. 9(a). However, no explosive spots and hence new detonative waves are observed, even under unstable propagation mode [50]. Therefore, the interactions between the blast waves and the deflagrative interface are expected to be significant in inducing the detonative pockets in RDC, including ignition of the shocked gas and determination of the propagation direction. In spite of the different origins, this counter-propagating blast waves essentially have the similar role of the reverse shock wave in formation of new detonation wavelets observed by Wang and his co-worker [40,41].

Plotted in Fig. 11 is the second representative event found in our simulations about initiating new detonative waves during the chaotic propagation stage, also through the time evolutions of temperature and pressure in the domain from Case 4. The reader should be reminded that in Fig. 11 the same numbers with S , E and D indicate that they share the same origin, although manifested in various forms from 10(a)–10(j), like shocks, explosive spots or detonation waves. At the beginning in Fig. 11(a), counter-rotating detonation waves $D2$ and $D3$ and a shock wave $S1$ (it is the blast wave from the triple point of $D2$) are seen. The counter-rotating detonation waves $D2$ and $D3$ in Fig. 11(b) are temporarily extinguished and degraded into strong shock waves $S2$ and $S3$ after they collide, which generates much higher local pressure in

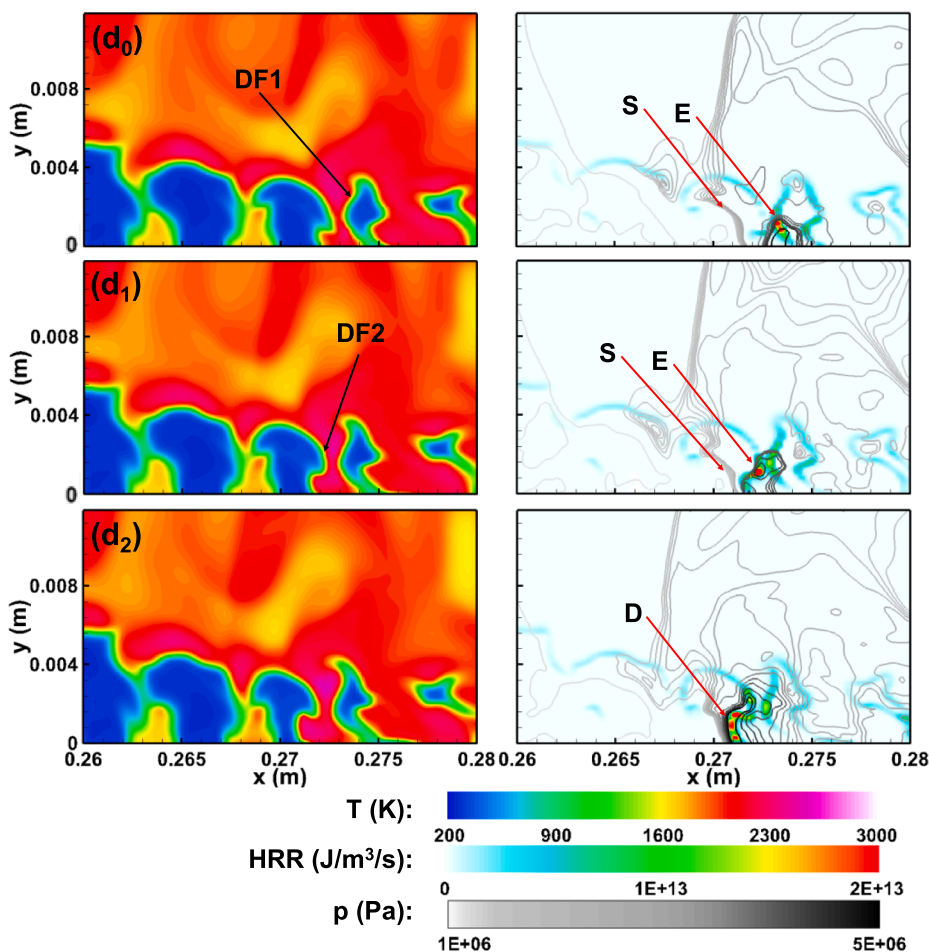


Fig. 10. Time sequences of temperature (left column) and heat release rate (right column) in chaotic propagation from Case 4. The pressure isolines are superimposed on the heat release rate contours. The first frame in (d_0) correspond to Fig. 9(d) and the time interval between two frames is 0.000001 s. The legend for S, D, E, DF same as that in Fig. 9.

Fig. 11(b). In Fig. 11(b), (c) and (d), no detonation waves exist in the RDE combustor, although the deflagrative combustion is still active along the contact surface. When the shock wave $S3$ arrives at the fresh reactant zone (approximately corresponding to the blue region in the left column), a local detonation wavelet (see its location through the pressure contours) happens near the injectors, which is marked as $D3$ as shown in Fig. 11(e). However, the detonation wave $D3$ degrades into a shock wave $S3$ again due to the insufficient reactants supply (see Fig. 11i), because $D1$ propagates ahead of $D3$, and therefore the post-detonation high pressure still suppresses the reactants injection, as indicated by Eq. (5).

For the shock waves $S1$ and $S2$, both experience the transition to detonation from the local deflagrative combustion, and new propagating detonation waves are formed as shown in Fig. 11(i) and (j), respectively. The detailed transition process, e.g. from $S1$ to $D1$, is shown from Fig. 12(e₀) to (e₂). In Fig. 12(e₀), a small high-pressure region (dark isolines in Fig. 12e₀) appears between the two peninsula-shaped deflagrative fronts $DF1$ and $DF2$. A local explosive spot can be observed at the concave section (with respect to the fresh gas) of $DF1$. This spot quickly expands along the $DF1$ deflagrative surface, and further intrigues strong heat release and pressure increase (see Fig. 12e₁). It gradually approaches the right propagating shock wave $S1$ and finally evolves into $D1$, as shown in Fig. 12(e₂). In front of the shock wave $S1$, sufficient reactants is available. For the shock wave $S2$, it evolves into $D2$ through the similar transients. Ultimately the detonative wave $D1$ and $D2$ is formed, as demonstrated in Fig. 11(f)–(j). The initiation of the hot spot frequently occurs in the entire chaotic propagation stage,

which can also be confirmed through the enhanced fluctuations of corresponding average HRR presented in Fig. 7(b).

In Fig. 10, the new detonation wave is developed from a hot spot along the interface (i.e. $DF1$ and $DF2$ in Fig. 10) between the newly injected reactants stream and the burned products. Differently, in Fig. 12, the explosive pocket is from the highly convoluted deflagrative surface (i.e. $DF1$ in Fig. 12). In the latter case, the residence time is longer, and hence the reactants gas near the hot spot (loosely corresponding to the blue areas in the temperature contours in Fig. 12) is expected to be better mixed with hot product gas, which would be more conducive for generation of the hot spot. Also, different from the results of Fig. 9, in Fig. 11, besides the blast wave $S1$, the shocks $S2$ and $S3$ are originally from the collision and extinction of two counter-rotating detonation waves. The sweeping of $S2$ and $S3$ directly leads to increased temperature and pressure behind them, where the formation of localized hot spots occurs, e.g. in Figs. 10 and 12. Therefore, based on our numerical experiments in Figs. 9–12, the interactions between shock waves (including the blast waves and degraded shocks from detonation wave collision) and deflagrative fronts (along the newly injected reactants stream and the contact surface) play a significant role in initiating multiple detonation waves during the chaotic propagation of RDWs.

The unsteady behaviors of shock waves during the chaotic RDW propagation can be further examined through the time series of the volume averaged pressure \bar{p} (scaled by the total pressure) in the reactants refill zone for Cases 1–6 in Fig. 13. Here \bar{p} is calculated from $\bar{p} = \int_{\Omega} P dv / \int_{\Omega} dv$, and Ω denotes the zones where $Y_{H_2} > 0$ holds. Recall

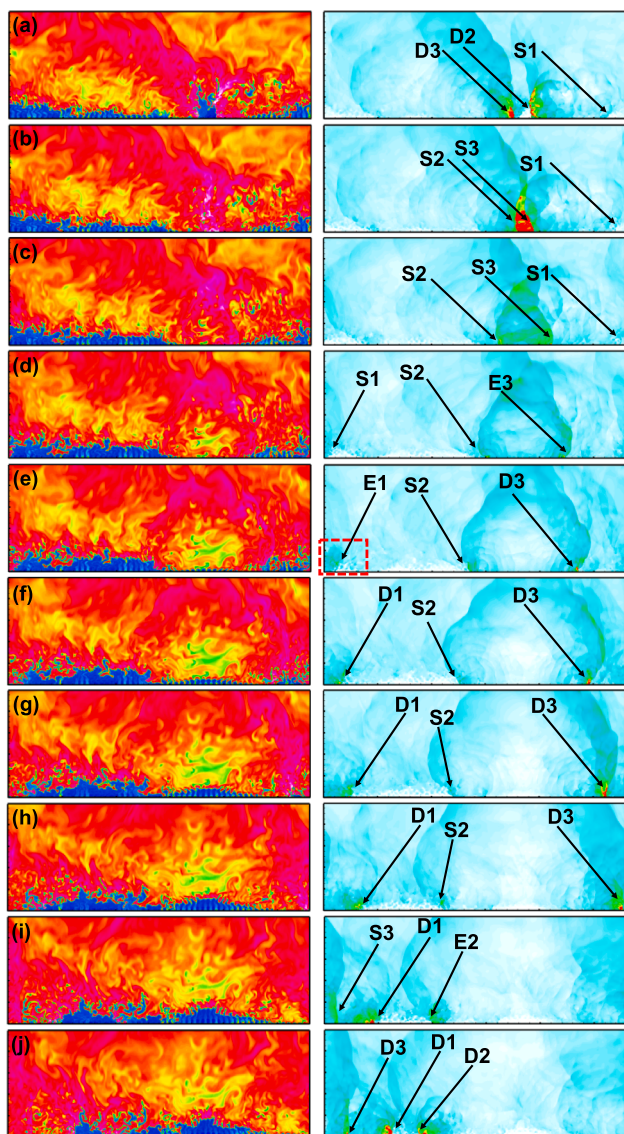


Fig. 11. Time sequences of temperature and pressure in chaotic propagation from Case 4. The time interval between two frames is 0.00001 s and the domain is 280 mm \times 100 mm. The legend for S, E and D same as that in Fig. 9. The numbers with S or D are used to identify the same wave (shock or detonation) in different instants.

that the total pressures in Cases 1–6 increase from $P_0 = 5$ to 30 atm. In general, for stable detonation propagation in all the cases, \bar{p}/P_0 is close to 0.4. Due to the increased P_0 , \bar{p} accordingly increases from Case 1 to 6. In addition, for cases without chaotic propagation, there are still some variations of the averaged pressure \bar{p} . For instance, in Case 2, between $0.002 \text{ s} < t < 0.0027 \text{ s}$, slight pressure increase (up to $0.1P_0$) can be seen. Its low magnitude fails to induce additional detonation initiation and therefore no shift between chaotic and stable propagation can be seen in Case 2, in line with the finding from Fig. 2. In Cases 4 and 5, there are two chaotic propagation period (e.g. $t < 0.0015 \text{ s}$ and $0.002 \text{ s} < t < 0.004 \text{ s}$ in Case 4, consistent with the results in Fig. 7), whereas in Case 6, only one chaotic period is seen. During the chaotic propagation stage, \bar{p} considerably increases: \bar{p}/P_0 first increases and then decreases to the stable value, i.e. around 0.4. The pressure increase in the chaotic RDW propagation period is caused by the intense shock waves in the reactants layer, as indicated above, which mainly result from the blast waves from the triple point and the detonation extinction. The frequent interactions between the shock wave and the

deflagration surface would lead to RDW re-initiation.

3.3. Numerical set-up effects on chaotic propagation prediction

The predictability of origin and chaotic propagation of multiple RDWs and their stabilization is of great importance to understand their underlying mechanisms and relevance to the practical rotating detonation dynamics [6]. As numerical experiments, prediction of this particular RDC dynamics may be influenced by the various aspects of numerical set-up, including initial and/or boundary conditions, mesh and chemical mechanism. Therefore, in this Section, we further perform supplementary numerical simulations, in order to confirm the observations from Section 3.2.

Fig. 14 shows the time series of the mass flow rate and volume averaged heat release rate when the total pressure P_0 is increased from 10 atm to 15 atm. Three instants are selected at 10 atm (from 0.001 s, 0.0015 s and 0.002 s, denoted as Cases 21, 22 and 23 in Fig. 14) as the initial fields for the current tests. Note that in the original field under 10 atm, only one detonation wave exists. For instance, in Case 21, the mass flow rate and averaged heat release rate experience the pronounced transient period after the total pressure is increased to 15 atm, which lasts 0.008 s or so. This corresponds to the chaotic RDW propagation, resulting in two new detonation waves. Then these two detonation waves stabilize, characterized by the relatively constant mass flow rate and heat release in Fig. 14. The results of two other initial fields in Case 22 and 23 are also shown in Fig. 14 and demonstrate qualitatively similar tendencies to that of Case 21. In all the numerical experiments shown in Fig. 14, two co-rotating detonative waves are found when the RDWs stably propagate. This is also observed in Case 3 (listed in Table 1) with the same total pressure, in which the detonation is initiated with hot spot and chaotic RDW propagation is also present. However, the propagation directions differ in these cases, although there is only one detonation wave in all the three initial fields.

Plotted in Fig. 15 are the time series of the mass flow rate and volume averaged heat release when we lower the total pressure from $P_0 = 10$ to 5 atm. Similar to Fig. 13, three initial fields from Case 2 are selected, i.e. $t = 0.001, 0.0015$ and 0.0015 s , termed as Cases 24, 25 and 26, respectively. Initially, there is only one detonative wave in all the three initial fields. A period of chaotic propagation occurs in Cases 24–26 from Fig. 15(a) before the stable propagation is established. In the stage of chaotic propagation, detonation quenching and re-initiation are observed. Different from the results in Fig. 14, here the RDC stabilizes with one detonative wave, which is in line with Case 1 ($P_0 = 5 \text{ atm}$) listed in Table 1.

Furthermore, in order to study the dependence of the findings in Sections 3.1 and 3.2 on the reaction mechanism and mesh resolution on RDW chaotic propagation modelling, based on Case 3, Case 31 with refined mesh (the minimal cell size is 0.05 mm) and Case 32 with one-step reaction mechanism (used in our previous study [50]) are performed (results not shown here), respectively. Similar phenomena, i.e. the chaotic propagation and multiple RDWs under high inlet total pressure, are also observed with finer mesh. However, these are not captured with global chemistry, which further confirms the necessity of the detailed mechanism in modelling unsteady RDC phenomena [4550].

Based on the numerical tests here and the results in Section 3.2, both stochastic and deterministic features in RDW chaotic propagation are observed. Generally, the stochasticity is related to when and where the explosive spot can be intrigued in the chaotic RDC field with complicated distributions of shock waves and combustion waves, how the new detonation waves can stabilize as well as their final propagation direction. Meanwhile, the deterministic features manifested from the above tests include the number of the stable RDWs under the same operating conditions (e.g. total pressure), irrespective of the initial fields. When the RDC is stable, its flow field becomes more organized and overall balance of the timescales is likely reached between various

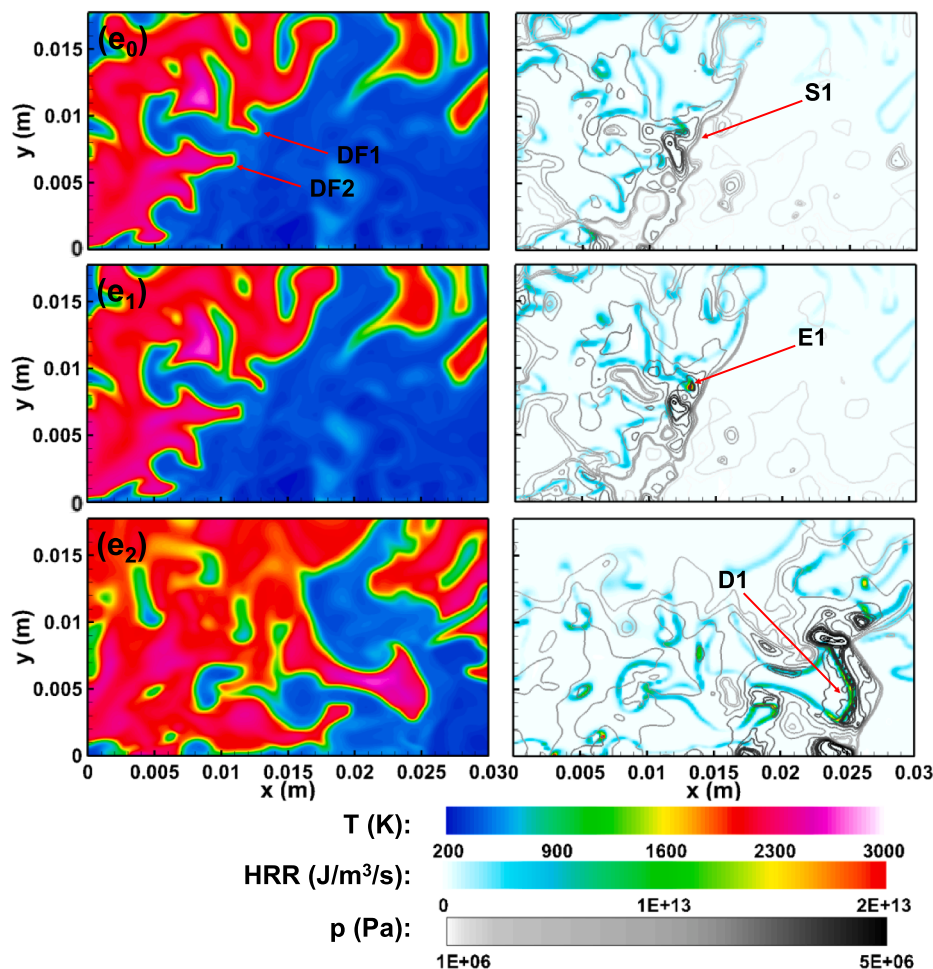


Fig. 12. Time sequences of temperature, pressure and heat release rate in chaotic propagation from Case 4. The first frame in (e_0) correspond to the red dashed box region in Fig. 11(e) and $t_{e1} = t_{e0} + 0.000001$ s, $t_{e2} = t_{e0} + 0.000002$ s. The legend for S, E and D same as that in Fig. 9. (For interpretation of the references to colour in this figure legend, the reader is referred to the web version of this article.)

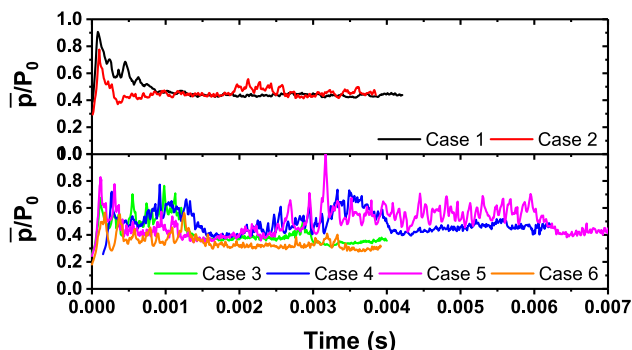


Fig. 13. Time history of volume averaged pressure (normalized by total pressure) in the reactants zones for Cases 1 ($P_0 = 5$ atm), 2 (10 atm), Case 3 (15 atm), Case 4 (20 atm), Case 5 (25 atm) and 6 (30 atm). Here $t = 0$ s corresponds to the ignition instant.

physic-chemical processes around or in the reactants refill zone, e.g. shock wave propagation, reactant mixing, autoignition, detonation, and deflagrative flame.

3.4. Fuel equivalence ratio effects on RDW propagation and bifurcation

In addition to the inlet total pressure, the effects of reactant equivalence ratio on the detonation propagation behavior are also studied. The cases within the detonable mixture fraction range of

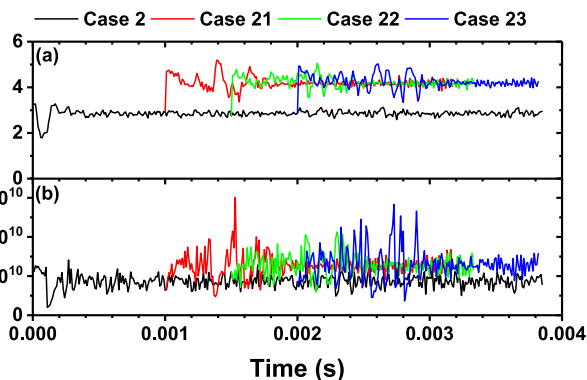


Fig. 14. Time history of (a) mass flow rate (in kg/s) and (b) volume averaged heat release rate (in $J/m^3/s$) when the inlet total pressure increases to 15 atm using three different fields under 10 atm as the initial conditions, corresponding to Cases 21, 22 and 23.

0.015–0.09 (the corresponding the equivalence ratio is 0.53 – 3.4) suggested by Glassman [77] are considered and simulated with different inlet total pressures, i.e. 5, 10, 15 and 20 atm. Fig. 16 shows the effects of reactant equivalence ratio and inlet total pressure on the detonation propagation behavior and velocity deficit. It can be found from Fig. 16(a) that the number of detonation wave is affected by the equivalence ratio and inlet total pressure within the detonable mixture fraction range. Stable detonation wave is obtained for near-

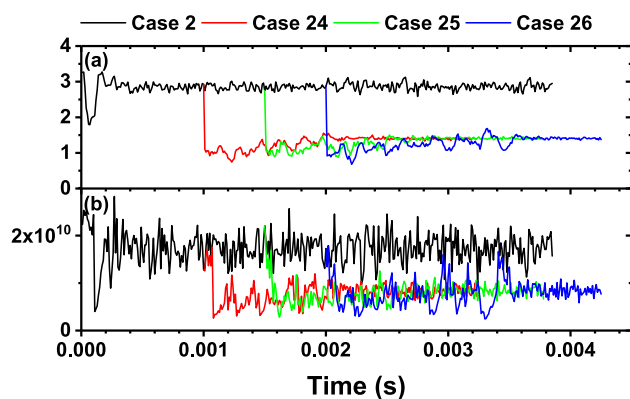


Fig. 15. Time history of (a) mass flow rate (in kg/s) and (b) volume averaged heat release rate (in $\text{J}/\text{m}^3/\text{s}$) when the inlet total pressure decreases to 5 atm using three different fields under 10 atm as the initial conditions, corresponding to Cases 24, 25 and 26.

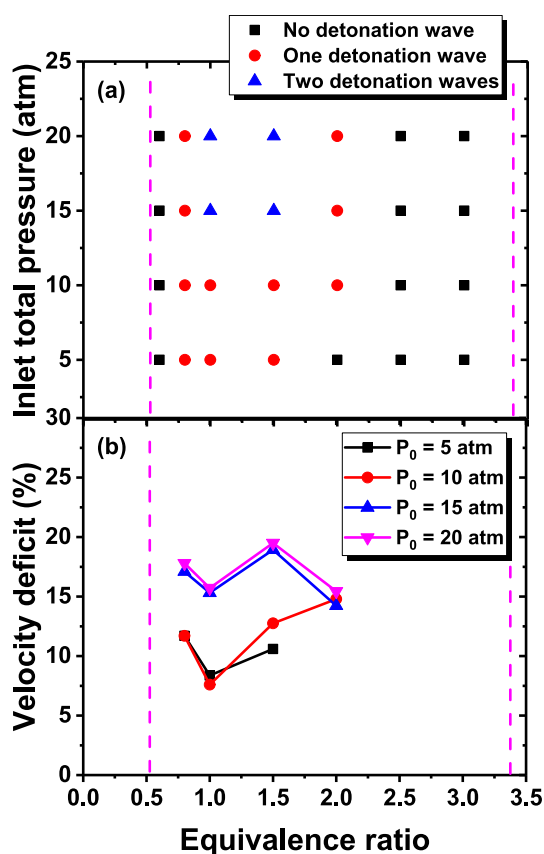


Fig. 16. Effects of equivalence ratio and inlet total pressure on the detonation propagation behavior and velocity deficit. The dashed lines represent detonable limits suggested by Glassman [77].

stoichiometric mixtures. Although the equivalence ratio of the mixture is in the detonable equivalence ratio range, the rotating detonation wave cannot be self-sustained in the modeled RDE combustor for the case with equivalence ratio greater than 2.0 or less than 0.8. Considering the spacing between injectors, the equivalence ratio for the cases without a self-sustained detonation wave may be out of the detonable range due to the mixing between the premixture and the burned gas. Two stable detonation waves are still obtained for the case with equivalence ratio of 1.5 and inlet total pressure greater than or equal to 15 atm. It should be noted that similar chaotic propagation as shown in Sections 3.1 and 3.2 would be observed for the case with two

detonation waves.

Furthermore, the velocity deficits for the cases with stable rotating detonation wave are calculated and shown in Fig. 16(b). The premixture with equivalence ratio of 1 would be completely consumed even if there exists mixing between the reaction products and fresh mixture and thus the rotating detonation wave of detonable mixture at equivalence ratio of 1 has the lowest velocity deficit for each inlet total pressure, especially for the case with inlet total pressure less than 15 atm. It has been suggested that the velocity deficit will be increased with increased detonation waves [34]. The cases with equivalence ratio of 1 and inlet total pressure of 15 and 20 atm have two stable detonation waves and the velocity deficit is almost twice of the case with one detonation wave. Therefore, in addition to the reactant mixing due to the discontinuous injection of the fresh reactants as suggested in Section 3.1, the fuel equivalence ratio may also be one of the reasons for the RDW velocity deficit.

4. Conclusions

The origin and chaotic propagation of multiple detonative waves in the two-dimensional modelled rotating detonation combustor fueled by premixed hydrogen/air mixtures are numerically investigated with detailed chemical mechanism. The arrangement of alternate reactants inlets and solid walls is adopted at the head end, to mimic the spatial non-uniformity of the propellant in the practical RDE combustor. A series of numerical experiments are performed through changing the inlet total pressures from 5 atm to 30 atm and the reactant equivalence ratios within the detonable equivalence ratio range.

It is found that higher total pressure leads to increased number of detonation waves when the RDC runs stably. When the total pressure is 5 and 10 atm, there is only one RDW. However, when it is beyond 10 atm, the number of co-rotating RDWs is increased to two in near-stoichiometric mixtures. Meanwhile, the propagation direction also differs for those cases with dual RDWs. For low total pressure with single RDW, no chaotic propagation transient after the detonation initiation is observed. Nevertheless, for high pressure situations, chaotic RDW propagation is present and lasts for a finitely long time before the RDC gets stabilized. The highly unsteady chaotic stage is characterized by frequent detonation extinction, re-ignition and re-orientation, irregular reactants refill zones, disorder flow fields and fluctuating performance indices (e.g. specific impulse, mass flow rate and heat release rate).

The results also show that the chaotic RDC stage is responsible for the variation of the RDW number and propagation direction. The explosive spots during chaotic stage result from the mutual enhancement between the travelling shock waves and the deflagrative fronts. Based on our numerical simulations, the shock waves are originally the blast waves irradiated from the triple point and the quenched counter-rotating RDWs due to their collisions. Meanwhile, the direction of the new detonation front is dominated by that of the shock waves. In addition, to achieve the self-sustaining propagation of new detonation waves, sufficient reactants should exist in front of the leading shock waves. Furthermore, from our numerical results, the final stabilization of the multiple RDWs depends on the appearance of the equally strong detonation waves and constant reactants supply in front of them.

The predictability of the chaotic RDW propagation is further discussed in terms of the influences of initial condition, mesh and chemical mechanism. In general, for the same total pressure conditions, the same RDW number is predicted when the RDC is stable, even if the different initial fields are adopted. However, different propagation directions are seen, which may be caused by the different direction of the explosive hot spots. Also, various mesh resolution would not qualitatively change the chaotic propagation transients. Furthermore, one-step chemical mechanism is used for comparisons, and the results show that no any explosive spots can arise and hence no chaotic RDW propagation is seen after the detonation is initiated.

In a practical RDE, combustion proceeds in highly turbulent flow field [6]. However, rotating detonative combustion is still an emerging research field and the state of the art is behind the research progress in low-speed turbulent combustion. Future work will be performed to examine the accuracy of the present modeling strategies (i.e. no models for turbulence and combustion) by comparisons with advanced turbulent combustion models such as probability density function method, flamelet and conditional moment closure models.

CRedit authorship contribution statement

Majie Zhao: Conceptualization, Methodology, Software, Writing - original draft, Formal analysis. **Huangwei Zhang:** Writing - review & editing, Supervision, Project administration.

Declaration of Competing Interest

The authors declare that they have no known competing financial interests or personal relationships that could have appeared to influence the work reported in this paper.

Acknowledgements

The numerical simulations were performed with the computational resources from National Supercomputing Center (NSCC), Singapore (<https://www.nscg.org/>).

References

- [1] Voitsekhozhskii BV. Stationary spin detonation. *Sov J Appl Mech Tech Phys* 1960;3:157–64.
- [2] Voitsekhozhskii BV, Mitrofanov VV, Topchiyan ME. Structure of the detonation front in gases (survey). *Combust Explos Shock Waves* 1969;5:267–73.
- [3] Lu, Frank K, Braun EM. Rotating detonation wave propulsion: experimental challenges, modeling, and engine concepts. *J Propuls Power* 2014;4:464–70.
- [4] Wolański P. Detonative propulsion. *Proc Combust Inst* 2013;34:125–58.
- [5] Zhou R, Wu D, Wang J. Progress of continuously rotating detonation engines. *Chinese J Aeronaut* 2016;29:15–29.
- [6] Anand V, Gutmark E. Rotating detonation combustors and their similarities to rocket instabilities. *Prog Energy Combust Sci* 2019;73:182–234.
- [7] Jourdaine N, Tsuboi N, Ozawa K, Kojima T, Hayashi AK. Three-dimensional numerical thrust performance analysis of hydrogen fuel mixture rotating detonation engine with aerospoke nozzle. *Proc Combust Inst* 2019;37:3443–51.
- [8] He W, Xie Q, Ji Z, Rao Z, Wang B. Characterizing continuously rotating detonation via nonlinear time series analysis. *Proc Combust Inst* 2019;37:3433–42.
- [9] Wang Y, Le J. Rotating detonation engines with two fuel orifice schemes. *Acta Astronaut* 2019;161:262–75.
- [10] Fang Y, Hu Z, Teng H. Numerical investigation of oblique detonations induced by a finite wedge in a stoichiometric hydrogen-air mixture. *Fuel* 2018;234:502–7.
- [11] Tian C, Teng H, Ng HD. Numerical investigation of oblique detonation structure in hydrogen-oxygen mixtures with Ar dilution. *Fuel* 2019;252:496–503.
- [12] Xiang G, Li H, Cao R, Chen X. Study of the features of oblique detonation induced by a finite wedge in hydrogen-air mixtures with varying equivalence ratios. *Fuel* 2020;264:116854.
- [13] Roy GD, Frolov SM, Borisov AA, Netzer DW. Pulse detonation propulsion: challenges, current status, and future perspective. *Prog Energy Combust Sci* 2004;30:545–672.
- [14] Kailasanath K. Recent developments in the research on rotating-detonation-wave engines. 55th AIAA Aerosp. Sci. Meet.; 2017.
- [15] Ng HD, Zhang F. Detonation instability. *Shock Waves Sci. Technol. Libr. Vol. 6*, Springer; 2012, p. 107–212.
- [16] Short M. A nonlinear evolution equation for pulsating Chapman-Jouguet detonations with chain-branching kinetics. *J Fluid Mech* 2001;430:381–400.
- [17] Short M, Sharpe GJ. Pulsating instability of detonations with a two-step chain-branching reaction model: theory and numerics. *Combust Theory Model* 2003;7:401–16.
- [18] Short M, Wang D. On the dynamics of pulsating detonations. *Combust Theory Model* 2001;5:343–52.
- [19] Radulescu MI, Lee JHS. The failure mechanism of gaseous detonations: experiments in porous wall tubes. *Combust Flame* 2002;131:29–46.
- [20] Zhang B, Liu H, Li Y. The effect of instability of detonation on the propagation modes near the limits in typical combustible mixtures. *Fuel* 2019;253:305–10.
- [21] Zhang B, Liu H, Yan B, Ng HD. Experimental study of detonation limits in methane-oxygen mixtures: determining tube scale and initial pressure effects. *Fuel* 2020;259:116220.
- [22] Zhang B, Liu H. Theoretical prediction model and experimental investigation of detonation limits in combustible gaseous mixtures. *Fuel* 2019;258:116132.
- [23] Bykovskii FA, Zhdan SA, Vedernikov EF. Continuous spin detonations. *J Propuls Power* 2006;22:1204–16.
- [24] Bykovskii FA, Zhdan SA, Vedernikov EF. Continuous spin detonation of fuel-air mixtures. *Combust Explos Shock Waves* 2006;42:463–71.
- [25] Kindracki J, Kobiera A, Wolański P, Gut Z, Foliński M, Swiderski K. Experimental and numerical study of the rotating detonation engine in hydrogen-air mixtures. *Prog Propuls Phys* 2011;2:555–82.
- [26] Sonwane C, Clafin S, Lynch E, Stout J. Recent advances in power cycles using rotating detonation engines with subcritical and supercritical CO₂. 4th Int. Symp. CO₂ Power Cycles, Pittsburgh, PA, 2014.
- [27] Liu SJ, Lin ZY, Liu WD, Lin W, Zhuang FC. Experimental realization of H₂/Air continuous rotating detonation in a cylindrical combustor. *Combust Sci Technol* 2012;184:1302–17.
- [28] Lentsch A, Bec R, Serre L, Falempin F, Daniau D, Piton D, et al. Overview of current French activities on PDRE and continuous detonation wave rocket engines. AIAA/CIRA 13th Int. Sp. Planes Hypersonics Syst. Technol. Conf., 2005, p. 3232.
- [29] Frolov SM, Aksenov VS, Ivanov VS, Medvedev SN, Shamshin IO. Flow Structure in Rotating Detonation Engine with Separate Supply of Fuel and Oxidizer: Experiment and CFD BT – Detonation Control for Propulsion: Pulse Detonation and Rotating Detonation Engines. In: Li J-M, Teo CJ, Khoo BC, Wang J-P, Wang C, editors., Cham: Springer International Publishing; 2018, p. 39–59.
- [30] Frolov SM, Aksenov VS, Ivanov VS, Shamshin IO. Large-scale hydrogen-air continuous detonation combustor. *Int J Hydrogen Energy* 2015;40:1616–23.
- [31] Deng L, Ma H, Xu C, Liu X, Zhou C. The feasibility of mode control in rotating detonation engine. *Appl Therm Eng* 2018;129:1538–50.
- [32] Anand V, George AS, Driscoll R, Gutmark E. Investigation of rotating detonation combustor operation with H₂-Air mixtures. *Int J Hydrogen Energy* 2016;41:1281–92.
- [33] St. George A, Driscoll R, Anand V, Gutmark E. On the existence and multiplicity of rotating detonations. *Proc Combust Inst* 2017;36:2691–8.
- [34] Rankin BA, Richardson DR, Caswell AW, Naples AG, Hoke JL, Schauer FR. Chemiluminescence imaging of an optically accessible non-premixed rotating detonation engine. *Combust Flame* 2017;176:12–22.
- [35] Suchocki J, Yu S-T, Hoke J, Naples A, Schauer F, Russo R. Rotating detonation engine operation. 50th AIAA Aerosp. Sci. Meet. Incl. new horizons forum Aerosp. Expo., 2012, p. 119.
- [36] Stechmann D, Heister SD, Sardeshmukh S. High-Pressure Rotating Detonation Engine Testing and Flameholding Analysis with Hydrogen and Natural Gas. 52nd AIAA/SAE/ASEE Jt. Propuls. Conf., American Institute of Aeronautics and Astronautics; 2016.
- [37] Roy A, Ferguson DH, Sidwell T, O'Meara B, Strakey P, Bedick C, et al. Experimental Study of Rotating Detonation Combustor Performance under Preheat and Back Pressure Operation. 55th AIAA Aerosp. Sci. Meet., American Institute of Aeronautics and Astronautics; 2017.
- [38] Liu S, Liu W, Lin Z, Lin W. Experimental Research on the propagation characteristics of continuous rotating detonation wave near the operating boundary. *Combust Sci Technol* 2015;187:1790–804.
- [39] Liu Y, Wang Y, Li Y, Li Y, Wang J. Spectral analysis and self-adjusting mechanism for oscillation phenomenon in hydrogen-oxygen continuously rotating detonation engine. *Chinese J Aeronaut* 2015;28:669–75.
- [40] Yao S, Wang J. Multiple ignitions and the stability of rotating detonation waves. *Appl Therm Eng* 2016;108:927–36.
- [41] Yao S, Liu M, Wang J. Numerical Investigation of spontaneous formation of multiple detonation wave fronts in rotating detonation engine. *Combust Sci Technol* 2015;187:1867–78.
- [42] Xia Z, Tang X, Luan M, Zhang S, Ma Z, Wang J. Numerical investigation of two-wave collision and wave structure evolution of rotating detonation engine with hollow combustor. *Int J Hydrogen Energy* 2018;43:21582–91.
- [43] Teng H, Zhou L, Yang P, Jiang Z. Numerical investigation of wavelet features in rotating detonations with a two-step induction-reaction model. *Int J Hydrogen Energy* 2020.
- [44] Schwer D, Kailasanath K. Feedback into mixture plenums in rotating detonation engines. 50th AIAA Aerosp. Sci. Meet. Incl. new horizons forum Aerosp. Expo., 2012, p. 617.
- [45] Sun J, Zhou J, Liu S, Lin Z, Cai J. Effects of injection nozzle exit width on rotating detonation engine. *Acta Astronaut* 2017;140:388–401.
- [46] Poling BE, Prausnitz JM, O'Connell JP. The properties of gases and liquids vol. 5. New York: McGraw-hill; 2001.
- [47] Jasak H. Error analysis and estimation for the finite volume method with applications to fluid flows; 1996.
- [48] Greenshields CJ, Weller HG, Gasparini L, Reese JM. Implementation of semi-discrete, non-staggered central schemes in a collocated, polyhedral, finite volume framework, for high-speed viscous flows. *Int J Numer Methods Fluids* 2010;63:1–21.
- [49] Huang Z, Zhao M, Zhang H. Modelling n-heptane dilute spray flames in a model supersonic combustor fueled by hydrogen. *Fuel* 2020;264:116809.
- [50] Zhao M, Li J-M, Teo CJ, Khoo BC, Zhang H. Effects of variable total pressures on instability and extinction of rotating detonation combustion. *Flow, Turbul Combust* 2020;104:261–90.
- [51] Kurganov A, Noelle S, Petrova G. Semidiscrete central-upwind schemes for hyperbolic conservation laws and hamilton-jacobi equations. vol. 23; 2001.
- [52] Bader G, Deuffhard P. A semi-implicit mid-point rule for stiff systems of ordinary differential equations. *Numer Math* 1983;41:373–98.
- [53] Sandu A, Verwer JG, Blom JG, Spee EJ, Carmichael GR, Potra FA. Benchmarking stiff ODE solvers for atmospheric chemistry problems II: Rosenbrock solvers. *Atmos*

- Environ 1997;31:3459–72.
- [54] Choi J-Y, Jeung I-S, Yoon Y. Computational fluid dynamics algorithms for unsteady shock-induced combustion, Part 1: validation. *AIAA J* 2000;38:1179–87.
- [55] Sato T, Voelkel S, Raman V. Detailed chemical kinetics based simulation of detonation-containing flows. *ASME Turbo Expo 2018 Turbomach. Tech. Conf. Expo., American Society of Mechanical Engineers*; 2018, p. V04AT04A063-V04AT04A063.
- [56] Qin Q, Zhang X. Study on the effects of geometry on the initiation characteristics of the oblique detonation wave for hydrogen-air mixture. *Int J Hydrogen Energy* 2019;44:17004–14.
- [57] Berglund M, Fedina E, Fureby C, Tegnér J, Sabel'Nikov V. Finite rate chemistry large-eddy simulation of self-ignition in supersonic combustion ramjet. *AIAA J* 2010;48:540–50.
- [58] Choi J-Y, Jeung I-S, Yoon Y. Computational fluid dynamics algorithms for unsteady shock-induced combustion, Part 2: comparison. *AIAA J* 2000;38:1188–95.
- [59] Liu P, Li Q, Huang Z, Zhang H. Interpretation of wake instability at slip line in rotating detonation. *ArXiv Prepr* 2018.
- [60] Li Q, Liu P, Zhang H. Further investigations on the interface instability between fresh injections and burnt products in 2-D rotating detonation. *Comput Fluids* 2018;170:261–72.
- [61] Schwer D, Kailasanath K. Numerical investigation of the physics of rotating-detonation-engines. *Proc Combust Inst* 2011;33:2195–202.
- [62] Yao SZS, Zhang MLL. Effects of injection conditions on the stability of rotating detonation waves. *Shock Waves* 2018;18:993–1009.
- [63] Bluemner R, Bohon M, Paschereit CO, Gutmark EJ. Dynamics of counter-rotating wave modes in an RDC. *2018 Jt Propuls Conf*; 2018.
- [64] Lin W, Zhou J, Liu S, Lin Z, Zhuang F. Experimental study on propagation mode of H₂/Air continuously rotating detonation wave. *Int J Hydrogen Energy* 2015;40:1980–93.
- [65] Fujii J, Kumazawa Y, Matsuo A, Nakagami S, Matsuoka K, Kasahara J. Numerical investigation on detonation velocity in rotating detonation engine chamber. *Proc Combust Inst* 2017;36:2665–72.
- [66] Hishida M, Fujiwara T, Wolanski P. Fundamentals of rotating detonations. *Shock Waves* 2009;19:1–10.
- [67] Tsuboi N, Watanabe Y, Kojima T, Hayashi AK. Numerical estimation of the thrust performance on a rotating detonation engine for a hydrogen–oxygen mixture. *Proc Combust Inst* 2015;35:2005–13.
- [68] Yi T-H, Lou J, Turangan C, Choi J-Y, Wolanski P. Propulsive performance of a continuously rotating detonation engine. *J Propuls Power* 2011;27:171–81.
- [69] Lawson J, Shepherd J. Shock & detonation toolbox installation instructions; 2019.
- [70] Bykovskii FA, Zhdan SA. Current status of research of continuous detonation in fuel-air mixtures (Review). *Combust Explos Shock Waves* 2015;51:21–35.
- [71] Rankin BA, Richardson DR, Caswell AW, Naples A, Hoke J, Schauer F. Imaging of OH* chemiluminescence in an optically accessible nonpremixed rotating detonation engine. *53rd AIAA Aerosp. Sci. Meet.*, 2015, p. 1604.
- [72] Xie Q, Wang B, Wen H, He W, Wolanski P. Enhancement of continuously rotating detonation in hydrogen and oxygen-enriched air. *Proc Combust Inst* 2019;37:3425–32.
- [73] Camargo A, Ng HD, Chao J, Lee JHS. Propagation of near-limit gaseous detonations in small diameter tubes. *Shock Waves* 2010;20:499–508.
- [74] Ishii K, Monwar M. Detonation propagation with velocity deficits in narrow channels. *Proc Combust Inst* 2011;33:2359–66.
- [75] Boeck LR, Berger FM, Hasslberger J, Sattelmayer T. Detonation propagation in hydrogen–air mixtures with transverse concentration gradients. *Shock Waves* 2016;26:181–92.
- [76] Katta VR, Cho KY, Hoke JL, Codoni JR, Schauer FR, Roquemore WM. Effect of increasing channel width on the structure of rotating detonation wave. *Proc Combust Inst* 2019;37:3575–83.
- [77] Glassman I, Yetter RA, Glumac NG. *Combustion*. Academic Press; 2014.